Journal of Circuits, Systems, and Computers

Gradient Guided Dual-Branch Network for Image Dehazing

Mingliang Gao

School of Electrical and Electronic Engineering,
Shandong University of Technology, Zibo, 255000, China

Qingyu Mao*

College of Electronics and Information Engineering,
Shenzhen University, Shenzhen, 518060, China

Qilei Li

School of Electronic Engineering and Computer Science,
Queen Mary University of London, London, E1 4NS, United Kingdom

Xiangyu Guo

School of Electrical and Electronic Engineering,
Shandong University of Technology, Zibo, 255000, China

Gwanggil Jeon

Department of Embedded Systems Engineering,
Incheon National University, Incheon, 22012, South Korea.

Recently, massive deep learning based image dehazing methods have sprung up. These methods can effectively remove most of the haze and obtain far better results than the traditional methods. With the removal of the haze, however, edge details of the image are also lost, which is usually more noticeable in the gradient space. This paper proposes a gradient guided dual-branch network (GGDB-Net) for image dehazing. Specifically, we explore the hazy image gradient map to guide our model to focus on the hazy regions and edge restoration. We implement two parallel branches with a comprehensive loss function, which collaborate to dehaze and repair the lost edges in haze images. Moreover, the gradient-guided approach can potentially be applied to existing learning-based image dehazing models to boost their performance. Experimental results indicate that our results have good visual perceptions and are comparable to state-of-the-art methods in quantitative metrics.

Keywords: Image dehazing; gradient guidance; edge restoration; dual-branch network.

1. Introduction

Due to the existence of various floating particles in the atmosphere, the outdoor images usually suffer from quality degradations, *e.g.,* color distortion, low contrast and

*Corresponding author: qingyu.mao@outlook.com

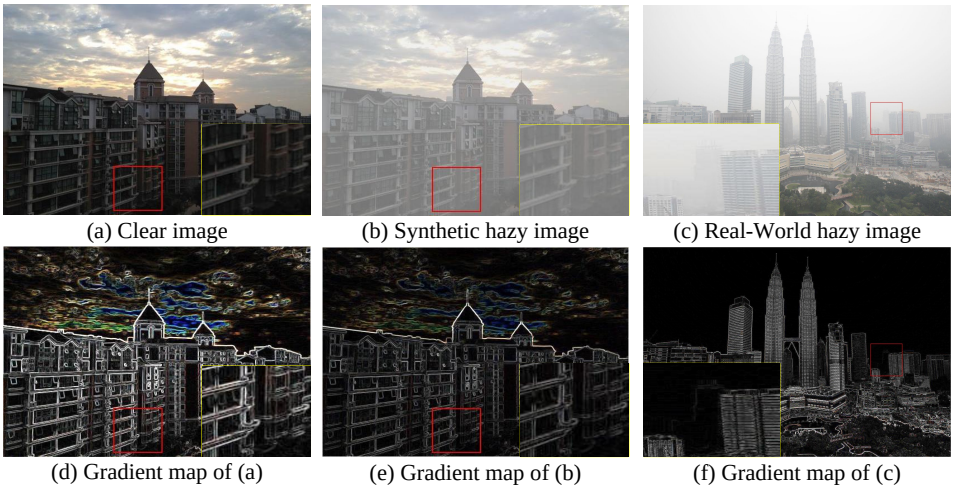

Fig. 1. Examples of images with the gradient maps.

edge blur The degradation causes detrimental impacts on subsequent visual-based analysis tasks, such as super-resolution [1,2], automatic drive [3,4], object detection[5,6], and Re-ID [7].

The hazy process is usually represented by a physical atmospheric scattering model [8,9], which can be written as:

$$I(x) = J(x)t(x) + A(1 - t(x)), \tag{1}$$

where $I(x)$ denotes the observed hazy image. $J(x)$ is the underlying haze-free scene, A and $t(x)$ represent the global atmosphere light and the medium transmission map, respectively. In this model, without the knowledge of A and $t(x)$, recovering $J(x)$ where only $I(x)$ is available is an ill-posed problem [10]. Based on the Eq. (1), many prior-based dahazing methods [11,12,13,14] utilized the statistics of clean images to estimate $t(x)$ and A. Although these priors improve the overall scene visibility somehow, their performance is not guaranteed in certain real cases [15]. For example, DCP [12] has bad performance in skies and snowy areas, since these areas do not meet the relative assumptions.

With the advances in deep learning, a number of deep learning based approaches have been employed in numerous computer vision tasks [16,17,18,19,15,20]. Meanwhile, various learning-based dehazing algorithms [21,22,23] were proposed to remove haze and reconstruct the haze-free image. In the early stage, the researchers attempt to use deep neural networks to estimate $t(x)$ and A, such as multi-scale CNN for image dehazing [22] and DehazeNet [21]. However, these methods may lead to large-scale reconstruction errors between the recovered image and the corresponding ground-truth, since the incorrect estimation on $t(x)$ and A.

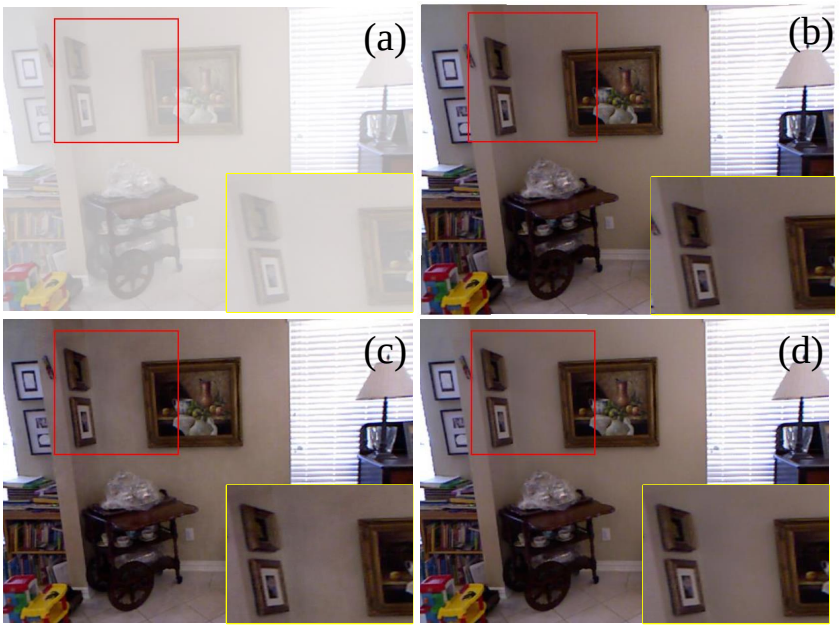

Fig. 2. Dehazing results. (a) a haze sample in SOTS, (b) the ground-truth, (c) result from FFA-Net and (d) our result. Our result are more natural and outperforms FFA-Net in detail.

Recently, several learning-based methods [10,24,25,26] applied CNN to predict haze-free images directly. These methods produce promising dehazing results with a significant improvement over the prior-based algorithms. However, when handling hazy images captured in heavy haze conditions, they are inability to eradicate haze while maintaining edge details effectively. This phenomenon can be attributed to the fact that some vital edge details are hidden under the haze, which overlaps with each other. They remove both the haze and edge details when processing the hazy image.

It is well known that image edge detail is obviously visible in the gradient map [27,28]. Some example images and their gradient maps are shown in Fig. 1. In Fig. 1(a) and (b), the edge detail in the clean image is significantly better than that in the hazy image. The edge details and haze overlap each other in image space and are hard to identify. Nevertheless, the edge detail is attenuated but not lost in the gradient space. Moreover, the region where the gradient intensity decay indicates the degradation level of haze influence.

To this end, we propose an end-to-end gradient guided dual-branch network (GGDB-Net), which succeeds in removing haze and restoring edge details simultaneously, as shown in Fig. 2. The contributions of the work are three-fold:

- We build a dual-branch parallel network called GGDB-Net for single image dehazing. The GGDB-Net divides the image dehazing into two subproblems, *i.e.,* haze removal and edge repair, which are processed separately on branches with different structures. The additional edge repair branch integrates the lost edge details to the final haze-free image.
- We apply the gradient map as additional information to the hazy image fed into the network. The gradient map guides the network to treat haze regions of different densities particularly. Moreover, the method is model-agnostic, which can be incorporated into other image dehazing methods to improve the performance.
- Experiments show that GGDB-Net achieve competitive performance, both qualitatively and quantitatively. Meanwhile, we investigate the effect of different gradient operators on image dehazing. Comprehensive ablation studies are also provided.

2. Related Work

Prior-based image dehazing methods assume statistical priors about clean images and use these priors as additional constraints to restore the information loss in the degradation procedure. The dark channel prior (DCP)[12] is a classical and wildly studied prior-based method. DCP assume the clean image with low intensity in at least one color channel, which reliably calculates $t(x)$. According to the assumption that the contrast of clear patch is higher than that of the hazy one, Tan *et al.* [14] maximize the local contrast of hazy images to estimate $t(x)$ by using Markov Random Field. Although these methods have been shown to be effective in removing haze, their performance is usually limited because the priors depend on the specific assumption and scene.

Learning-based image dehazing methods has attracted extensive attention of computer vision researchers, which benefits from the large scale benchmark datasets and the powerful ability of deep tools. Early researchers attempted to use CNNs to predict $t(x)$ and A for recovering the haze-free image, such as multi-scale CNN [22] and DehazeNet [21]. Chen *et al.* [25] designed a gated-fusion network by fusing different level features to reconstruct the finer haze-free image . Bianco *et al.* [26] adopted an encoder-decoder structure and added the perceptual loss to promote local consistency for image dehazing. Qin *et al.* [10] designed an feature fusion attention network (FFA-Net) to build the high-quality haze-free image. Although these learning-based methods improve the overall visual quality, they still lose a certain extent of edge details when removing the haze.

Gradient information has been utilized in several previous low-level computer vision problems [28,29]. For the image dehazing task, Singh *et al.* [30] use gradient prior to first estimate $t(x)$ and A and then refine $t(x)$ by the gradient map. Ye *et al.* [31] proposed a novel color-line prior method, which use gradient information to control the structural similarity of haze-free images and avoid the halo effect. In

these methods, they use gradient information as prior knowledge to estimate $t(x)$. However, their procedure of estimating $t(x)$ is not robust and inefficient.

Although CNN is prominent in transforming pixels distribution and feature extraction, few dehaze methods have combined gradient information with deep tools. Dong *et al.* [24] proposed a GAN model with fusion-discriminator (FD-GAN) to recover the haze-free image, which extract high-frequency (an alternative representation similar to gradient information) and low-frequency components into the discriminator. However, the influence of the discriminator on the generator is unstable, and the generator cannot exploit the local gradient information to improve haze removal. Ma *et al.* [28] added a collateral gradient branch and used gradient loss as additional constraint to control the structure preservation in SR image. Their method which named Structure-preserving super resolution (SPSR), used the difference between adjacent pixels to calculate the low-resolution (LR) gradient map, but this is problematic in the hazy image. We describe more details in the experimental section. Inspired by SPSR [28] and FD-GAN [24], we propose a dual-branch gradient information guided image dehazing network, which aims to remove haze while maintaining edge details.

3. Method

3.1. *Overview*

An overview of the proposed GGDB-Net is depicted in Fig. 3, which composes of haze removal branch, edge repair branch, and feature fusion module.

To be concrete, the haze removal branch G_{haze} takes the concatenated I^{cat} of the hazy image I^{haze} and its gradient map I^{haze}_{gra} as input and aims to eradicate haze. I^{cat} is the input to the edge repair branch G_{edge}, which focuses on repairing edge details. The feature fusion module M_{fusion} integrates features from G_{haze} and G_{edge} to obtain the final haze-free image I^{hf}. This procedure can be written as:

$$I^{hf} = M_{fusion}\Big(cat\big(G_{haze}(I^{cat}), G_{edge}(I^{cat})\big)\Big), \tag{2}$$

where $cat(\cdot)$ indicates the concatenate operation. In particular, the gradient images I_{gra} are obtained by the Sobel operator [32]:

$$I_{gra} = \left\| Sobel_x(I)^2 + Sobel_y(I)^2 \right\|_2, \tag{3}$$

where I is the original image in the training dataset or test dataset. $Sobel_x(\cdot)$ and $Sobel_y(\cdot)$ are the Sobel operators in the horizontal and vertical directions, respectively.

3.2. *Details in Architecture*

Haze Removal Branch: We design a haze removal branch G_{haze} to remove haze altogether based on U-Net [33]. This architecture reduces the parameters in the module and extracts multi-scale features. We set a convolutional layer with Sobel

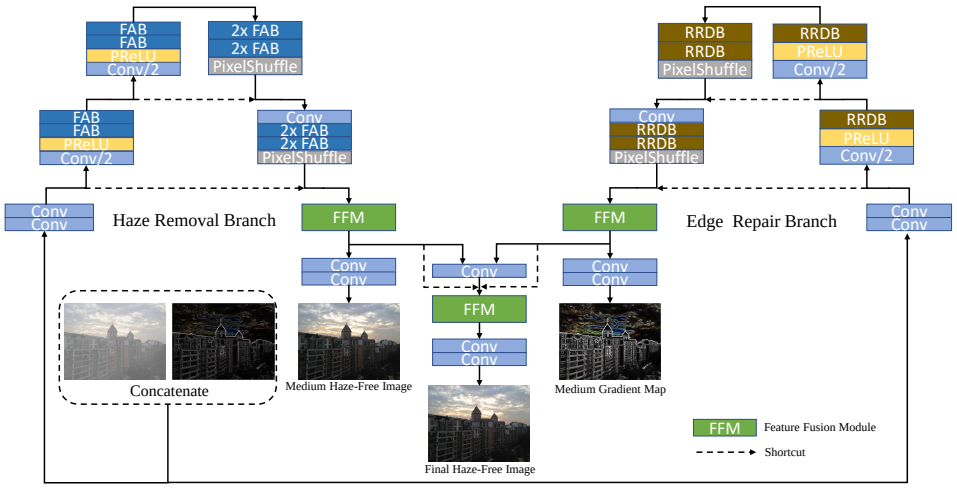

Fig. 3. Overview of the proposed GGDB-Net.

operator to get I_{gra}^{haze} and concatenate with I^{haze} firstly. Then the low-level features of I^{cat} are extracted by two convolutional layers. The feature attention block (FAB) [10] contains local residual learning and feature attention. Specifically, the feature attention combines channel attention [34] with pixel attention, and it enables the network to pay more attentions on more important features and pixels regions. Two FABs are added to the back of each downsample layer, and four FABs in front of each upsample layer to integrate features further. To avoid losing image information and effectively using low-level features, we concatenate the same-scale features to subsequent convolutional layers and FABs. Finally, we feed the feature maps to the feature fusion module. Meanwhile, the feature maps are also used to generate medium haze-free images by two 3×3 convolutional layers.

Edge Repair Branch: Similar to the haze removal branch, the edge repair branch consists of convolutional layers, downsample layer, upsample layer, and residual-in-residual dense block (RRDB) [35]. Considering the RRDB has far more parameters and convolutional layers than the FAB, we only use one RRDB in each position. Unlike the haze removal network, we expect the output of the edge repair branch to approximate the gradient map of haze-free images.

Feature Fusion Module: The feature fusion module is also adopted in the tail of the above two branches. Details and implementation can be found in FFA-Net[10]. Here, we refer specifically to the tail part of the whole GGDB-Net, which concatenates feature maps of the two branches to reconstruct the final haze-free image. We denote channel-attention as CA and pixel-attention as PA. The shape of regular feature maps is $C \times H \times W$.

$$F_{ca} = CA\big(cat(F_{haze}, F_{edge})\big), \tag{4}$$

where F_{haze} and F_{edge} denote the feature maps of the two branches feeding into the feature fusion module. and F_{ca} is the output of channel-attention layer and has a shape of $2C \times 1 \times 1$. Then, F_{ca} is element-wise multiplied by F_{haze} and F_{edge}.

$$F_{pa} = PA\big(F_{ca}[:C,:,:] \otimes F_{haze} + F_{ca}[C:,:,:] \otimes F_{edge}\big), \tag{5}$$

where F_{pa} is the out of pixel-attention layer, and $\otimes$ is the element-wise multiplication. F_{pa} feed into two convolutional layers to reconstructed the final haze-free image.

In order to get satisfactorily clean image in a multi-supervised progressive manner, we design a comprehensive loss function for the intermediate and final outputs.

3.3. *Comprehensive Loss Function*

To enable the model to progressively reconstruct haze-free image satisfactorily with multi-supervision, we design the loss function from two different perspectives. The proposed GGDB-Net have three output which are the medium haze-free image, the medium gradient map, and the final haze-free image. Therefore, one loss function cannot constrain the output of model effectively. The loss of pixel space is denoted as follows:

$$L_{mid}^{pix} = \frac{1}{N}\sum_{i=1}^{N} \left\| I^{gt} - G_{haze}(I^{cat}) \right\|_1, \tag{6}$$

$$L_{final}^{pix} = \frac{1}{N}\sum_{i=1}^{N} \left\| I^{gt} - I^{hf} \right\|_1, \tag{7}$$

where I^{gt} is the ground-truth clean image. To maintain the edge details in the final haze-free image, we design a gradient loss to achieve the goal. The loss of gradient space is described as:

$$L_{mid}^{gra} = \frac{1}{N}\sum_{i=1}^{N} \left\| Sobel(I^{gt}) - G_{edge}(I^{cat}) \right\|_1, \tag{8}$$

$$L_{final}^{gra} = \frac{1}{N}\sum_{i=1}^{N} \left\| Sobel(I^{gt}) - Sobel(I^{hf}) \right\|_1, \tag{9}$$

where $Sobel(\cdot)$ is the Sobel operation which same as the Eq. (3). It is worth noting that we transform *Sobel* into a convolutional layer with fixed parameters. Hence, the model can be trained in an end-to-end manner. The total loss function is formulated:

$$Loss_{total} = L_{mid}^{pix} + \alpha L_{final}^{pix} + \beta L_{mid}^{gra} + \gamma L_{final}^{gra}, \tag{10}$$

where α, β and γ are the trade-off weights.

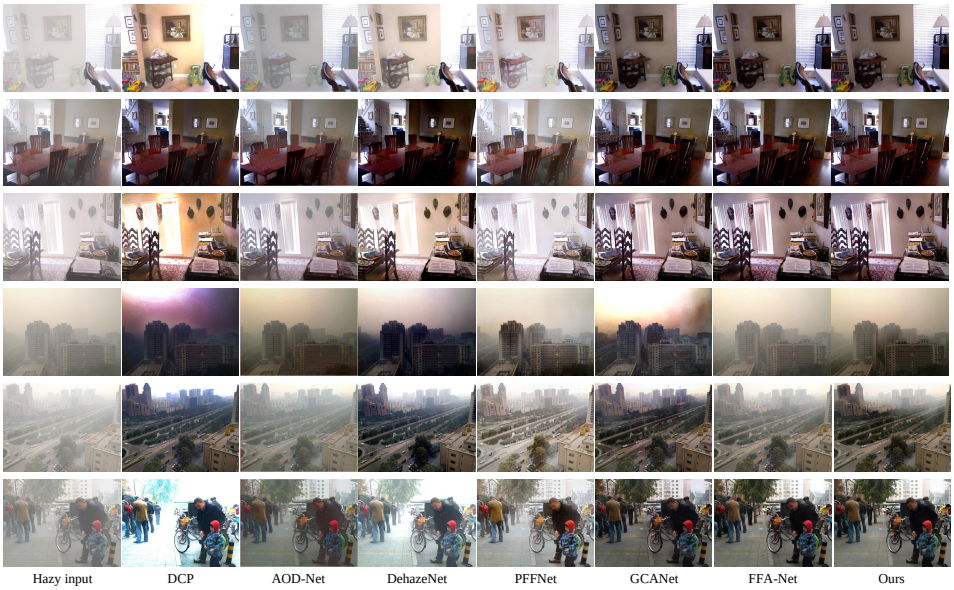

Fig. 4. Visual comparisons on indoor and outdoor environments for SOTS dataset.

4. Experiments

4.1. *Datasets*

The RESIDE [36] dataset is a widely used benchmark dataset for image dehazing, which consists of Indoor Training Set (ITS, with 13,990 image pairs) and Outdoor Training Set (OTS, with 60,246 image pairs). Meanwhile, we introduce the synthetic datasets and real-world datasets to validate the dehazing performance of the GGDB-Net to ensure the completeness. The Synthetic Objective Testing Set (SOTS) of RESIDE is adopted for performance evaluation. We also test on several well-known real-world datasets for qualitative assessment, including O-HAZE [37] and I-HAZE [38].

4.2. *Implementation Details*

During the training process, the training set is first randomly flipped horizontally and vertically. Then, they are randomly cropped to 240×240. Finally, the pair of image patches as inputs and feed into GGDB-Net. The Adam optimizer is adopted and $\beta_1 = 0.9$ and $\beta_2 = 0.999$. The trade-off weights in loss function are set to $\alpha = 0.01$, $\beta = 0.01$ and $\gamma = 10$, respectively.

For ITS and OTS datasets, we train the GGDB-Net for 3×10^5 and 6×10^5 steps with batch size of 6, respectively. The learning rate is initially set to 1×10^{-4} and 5×10^{-5}, and the cosine annealing strategy [39] is adopted to control the learning

rate. All experiments are implemented on PyTorch [40] with an NVIDIA RTX 2080Ti GPU.

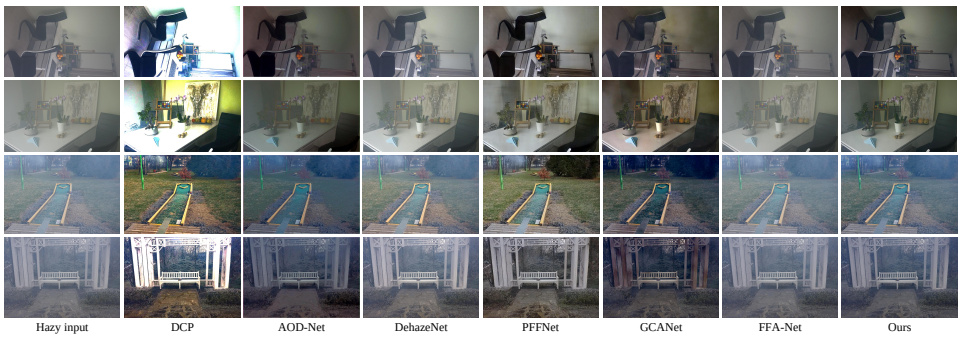

Fig. 5. Visual comparisons on I-HAZE and O-HAZE datasets

4.3. *Evaluation and Results*

We compare the GGDB-Net with six state-of-the-art (SOTA) methods, *i.e.,* one traditional method DCP [12], and five learning-based methods, i.e., AOD-Net [41], DehazeNet [21], GCANet [25], FFA-Net [10], and PFFNet [42]. Two evaluation metrics,*i.e.,* PSNR and SSIM [43] are adopted. Comparative results are referred in Table 1.

The proposed GGDB-Net outperforms other SOTA competitors by a large margin in PSNR and SSIM. Compare with the FFA-Net [10] which ranks the second place, GGDB-Net achieves 1.44dB PSNR and 0.029 SSIM gain in SOTS indoor. Qualitative comparison results are illustrated in Fig. 4 and Fig. 5. The results of DCP and DehazeNet with excessive brightness relative to others. AOD-Net and PFFNet fail to get rid of the haze entirely, and they are suffered from color distortion. GCANet and FFA-Net lose edge details and have in-homogeneous illuminations. In contrast, the proposed GGDB-Net generate more natural results with apparent edges and smoother illumination.

4.4. *Ablation Study*

To explore the validity of the GGDB-Net, it is necessary to present an ablation study by validating different parts in the GGDB-Net.

Ablation Study on Different Components: In this subsection, all experiments are trained by ITS and tested on SOTS with the same parameters of our implementation details, excepting that the training iterations is set to 2×10^5. The results are shown in Table 2. By removing the gradient map and using the haze image alone as input, the value of PSNR drops from 35.1846 to 33.2488, which

Table 1. Quantitative comparisons on SOTS.

Method	SOTS indoor		SOTS outdoor	
	PSNR	SSIM	PSNR	SSIM
DCP [12]	16.6240	0.8183	21.1532	0.8958
AOD-Net [41]	20.8582	0.8790	23.3615	0.9170
DehazeNet [21]	22.3024	0.8805	21.5538	0.8441
PFFNet [42]	29.5132	0.9560	25.8016	0.8928
GCANet [25]	30.1340	0.9672	28.3426	0.9468
FFA-Net [10]	36.3870	0.9886	33.5723	0.9840
GGDB-Net(Ours)	**37.8351**	**0.9915**	**34.4930**	**0.9855**

Table 2. Ablation study of the GGDB-Net.

Haze removal branch	✓	✓	✓	✓
Edge rapair branch		✓	✓	✓
Gradient-guided			✓	✓
Gradient loss				✓
PSNR	32.5907	33.2488	34.5658	**35.1846**
SSIM	0.9820	0.9837	0.9862	**0.9876**

proves that the gradient guidance is helpful for image dehazing. We can also see that even we only use the haze removal branch, both PSNR and SSIM have declined significantly. Moreover, the impacts of medium losses are also investigated.

Ablation Study on Different Gradient Operators: In this part, we perform experiments to demonstrate the effect of several commonly gradient operators on our GGDB-Net. Comparative results are depicted in Table 2. It shows that the Sobel operator suits best among all the other operators. Since the edge details in haze images are hidden under the haze, small extraction factors cannot extract significant edges for guiding haze removals, such as Difference and Laplace operator. In contrast, the Scharr operator uses too large extraction factors, which introduces enormous noise in the background and around objects, causing instability and deterioration of our model. Finally, we can observe that the Sobel operator both extracts sufficient features and avoids the noise problem. Thus, we apply the Sobel operator to get gradient maps.

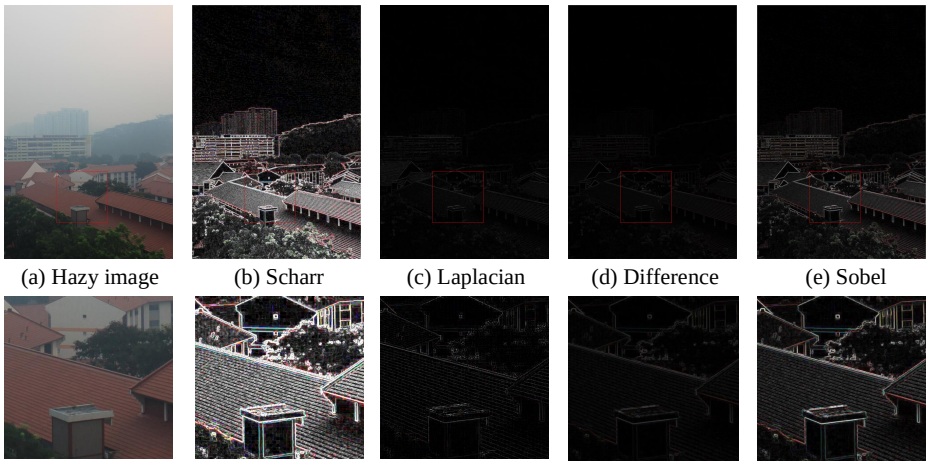

Fig. 6. Visual comparison of different gradient operators.

Table 3. Ablation study of different gradient operators.

Method	PSNR	SSIM
Scharr operator	16.3393	0.4491
Differential operator	34.3495	0.9857
Laplace operator	34.6373	0.9871
Sobel operator	**35.1846**	**0.9876**

5. Conclusion

We propose a gradient guided dual-branch network (GGDB-Net) for single image dehazing in this work. The key idea is to decouple the haze removal and edge repair with dual parallel branches and use the gradient map to guide the model to focus on haze and edge. With the aid of gradient information, guidance can also be used in other models to enhance the performance of image dehazing. Moreover, we analyse the effect of different gradient operators for image dehazing. Experimental results prove that the GGDB-Net performs favourably against the state-of-the-arts methods, and it is qualified to get rid of remove the uneven haze and recover edge details for real haze images.

Acknowledgements

This work is supported by the National Natural Science Foundation of China (Nos.61601266) and National Natural Science Foundation of Shandong Province (ZR2020MF127).

References

1. Q. Li, Z. Li, L. Lu, G. Jeon, K. Liu and X. Yang, Gated multiple feedback network for image super-resolution, *arXiv preprint arXiv:1907.04253* (2019).
2. J. Wang, J. Wu, Z. Wu, M. Anisetti and G. Jeon, Bayesian method application for color demosaicking, *Optical Engineering* **57**(5) (2018) p. 053102.
3. F. Ding, K. Yu, Z. Gu, X. Li and Y. Shi, Perceptual enhancement for autonomous vehicles: restoring visually degraded images for context prediction via adversarial training, *IEEE Transactions on Intelligent Transportation Systems* (2021).
4. G. Jeon, S.-J. Park, Y. Fang, M. Anisetti, V. Bellandi, E. Damiani and J. Jeong, Specification of efficient block-matching scheme for motion estimation in video compression, *Optical Engineering* **48**(12) (2009) p. 127005.
5. F. Ding, G. Zhu, M. Alazab, X. Li and K. Yu, Deep-learning-empowered digital forensics for edge consumer electronics in 5g hetnets, *IEEE consumer electronics magazine* (2020).
6. Z. Guo, K. Yu, A. Jolfaei, F. Ding and N. Zhang, Fuz-spam: label smoothing-based fuzzy detection of spammers in internet of things, *IEEE Transactions on Fuzzy Systems* (2021).
7. Q. Li, J. Huang and S. Gong, Local-global associative frame assemble in video re-id, *arXiv preprint arXiv:2110.12018* (2021).
8. E. J. McCartney, Optics of the atmosphere: scattering by molecules and particles, *nyjw* (1976).
9. S. G. Narasimhan and S. K. Nayar, Vision and the atmosphere, *International journal of computer vision* **48**(3) (2002) 233–254.
10. X. Qin, Z. Wang, Y. Bai, X. Xie and H. Jia, Ffa-net: Feature fusion attention network for single image dehazing., in *AAAI*, 2020, pp. 11908–11915.
11. R. Fattal, Dehazing using color-lines, *ACM transactions on graphics (TOG)* **34**(1) (2014) 1–14.
12. K. He, J. Sun and X. Tang, Single image haze removal using dark channel prior, *IEEE transactions on pattern analysis and machine intelligence* **33**(12) (2010) 2341–2353.
13. Q. Zhu, J. Mai and L. Shao, A fast single image haze removal algorithm using color attenuation prior, *IEEE transactions on image processing* **24**(11) (2015) 3522–3533.
14. R. T. Tan, Visibility in bad weather from a single image, in *2008 IEEE Conference on Computer Vision and Pattern Recognition*, IEEE2008, pp. 1–8.
15. B. Li, Z. Peng, P. Hou, M. He, M. Anisetti and G. Jeon, Reliability and capability based computation offloading strategy for vehicular ad hoc clouds, *Journal of cloud computing* **8**(1) (2019) 1–14.
16. Q. Li, L. Lu, Z. Li, W. Wu, Z. Liu, G. Jeon and X. Yang, Coupled gan with relativistic discriminators for infrared and visible images fusion, *IEEE Sensors Journal* **21**(6) (2019) 7458–7467.
17. K. Yu, L. Tan, L. Lin, X. Cheng, Z. Yi and T. Sato, Deep-learning-empowered breast cancer auxiliary diagnosis for 5gb remote e-health, *IEEE Wireless Communications* **28**(3) (2021) 54–61.
18. F. Ding, G. Zhu, Y. Li, X. Zhang, P. K. Atrey and S. Lyu, Anti-forensics for face swapping videos via adversarial training, *IEEE Transactions on Multimedia* (2021).
19. K. Yu, L. Tan, S. Mumtaz, S. Al-Rubaye, A. Al-Dulaimi, A. K. Bashir and F. A. Khan, Securing critical infrastructures: Deep-learning-based threat detection in iiot, *IEEE Communications Magazine* **59**(10) (2021) 76–82.
20. J. Zhang, K. Yu, Z. Wen, X. Qi and A. K. Paul, 3d reconstruction for motion blurred images using deep learning-based intelligent systems, *CMC-computers Materials & Continua* **66**(2) (2021) 2087–2104.

21. B. Cai, X. Xu, K. Jia, C. Qing and D. Tao, Dehazenet: An end-to-end system for single image haze removal, *IEEE Transactions on Image Processing* **25**(11) (2016) 5187–5198.
22. W. Ren, S. Liu, H. Zhang, J. Pan, X. Cao and M.-H. Yang, Single image dehazing via multi-scale convolutional neural networks, in *European conference on computer vision*, Springer2016, pp. 154–169.
23. H. Zhang and V. M. Patel, Densely connected pyramid dehazing network, in *Proceedings of the IEEE conference on computer vision and pattern recognition*, 2018, pp. 3194–3203.
24. Y. Dong, Y. Liu, H. Zhang, S. Chen and Y. Qiao, Fd-gan: Generative adversarial networks with fusion-discriminator for single image dehazing., in *AAAI*, 2020, pp. 10729–10736.
25. D. Chen, M. He, Q. Fan, J. Liao, L. Zhang, D. Hou, L. Yuan and G. Hua, Gated context aggregation network for image dehazing and deraining, in *2019 IEEE Winter Conference on Applications of Computer Vision (WACV)*, IEEE2019, pp. 1375–1383.
26. S. Bianco, L. Celona, F. Piccoli and R. Schettini, High-resolution single image dehazing using encoder-decoder architecture, in *Proceedings of the IEEE Conference on Computer Vision and Pattern Recognition Workshops*, 2019, pp. 0–0.
27. J. Chen, L. Zhang, L. Lu, Q. Li, M. Hu and X. Yang, A novel medical image fusion method based on rolling guidance filtering, *Internet of Things* **14** (2021) p. 100172.
28. C. Ma, Y. Rao, Y. Cheng, C. Chen, J. Lu and J. Zhou, Structure-preserving super resolution with gradient guidance, in *Proceedings of the IEEE/CVF Conference on Computer Vision and Pattern Recognition*, 2020, pp. 7769–7778.
29. K. Nazeri, E. Ng, T. Joseph, F. Z. Qureshi and M. Ebrahimi, Edgeconnect: Generative image inpainting with adversarial edge learning, *arXiv preprint arXiv:1901.00212* (2019).
30. D. Singh, V. Kumar and M. Kaur, Single image dehazing using gradient channel prior, *Applied Intelligence* **49**(12) (2019) 4276–4293.
31. D. Ye and R. Yang, Gradient information-orientated colour-line priori knowledge for remote sensing images dehazing, *Sensing and Imaging* **21**(1) (2020) 1–17.
32. R. O. Duda, P. E. Hart *et al.*, *Pattern classification and scene analysis* (Wiley New York, 1973).
33. O. Ronneberger, P. Fischer and T. Brox, U-net: Convolutional networks for biomedical image segmentation, in *International Conference on Medical image computing and computer-assisted intervention*, Springer2015, pp. 234–241.
34. Y. Zhang, K. Li, K. Li, L. Wang, B. Zhong and Y. Fu, Image super-resolution using very deep residual channel attention networks, in *Proceedings of the European Conference on Computer Vision (ECCV)*, 2018, pp. 286–301.
35. X. Wang, K. Yu, S. Wu, J. Gu, Y. Liu, C. Dong, Y. Qiao and C. Change Loy, Esrgan: Enhanced super-resolution generative adversarial networks, in *Proceedings of the European Conference on Computer Vision (ECCV)*, 2018, pp. 0–0.
36. B. Li, W. Ren, D. Fu, D. Tao, D. Feng, W. Zeng and Z. Wang, Benchmarking single-image dehazing and beyond, *IEEE Transactions on Image Processing* **28**(1) (2018) 492–505.
37. C. O. Ancuti, C. Ancuti, R. Timofte and C. D. Vleeschouwer, O-haze: a dehazing benchmark with real hazy and haze-free outdoor images, in *IEEE Conference on Computer Vision and Pattern Recognition, NTIRE Workshop*, *NTIRE CVPR'18*2018.
38. C. O. Ancuti, C. Ancuti, R. Timofte and C. D. Vleeschouwer, I-haze: a dehazing benchmark with real hazy and haze-free indoor images, in *arXiv:1804.05091v1*, 2018.
39. T. He, Z. Zhang, H. Zhang, Z. Zhang, J. Xie and M. Li, Bag of tricks for image clas-

sification with convolutional neural networks, in *Proceedings of the IEEE Conference on Computer Vision and Pattern Recognition*, 2019, pp. 558–567.
40. A. Paszke, S. Gross, S. Chintala, G. Chanan, E. Yang, Z. DeVito, Z. Lin, A. Desmaison, L. Antiga and A. Lerer, Automatic differentiation in pytorch (2017).
41. B. Li, X. Peng, Z. Wang, J. Xu and D. Feng, Aod-net: All-in-one dehazing network, in *Proceedings of the IEEE international conference on computer vision*, 2017, pp. 4770–4778.
42. K. Mei, A. Jiang, J. Li and M. Wang, Progressive feature fusion network for realistic image dehazing, in *Asian conference on computer vision*, Springer2018, pp. 203–215.
43. Z. Wang, A. C. Bovik, H. R. Sheikh and E. P. Simoncelli, Image quality assessment: from error visibility to structural similarity, *IEEE transactions on image processing* **13**(4) (2004) 600–612.